AMERICAN SOCIETY FOR MICROBIOLOGY | Applied and Environmental Microbiology®

ENVIRONMENTAL MICROBIOLOGY

Functional Determinants of Extracellular Polymeric Substances in Membrane Biofouling: Experimental Evidence from Pure-Cultured Sludge Bacteria

Naga Raju Maddela,[a,b] Zhongbo Zhou,[a,b] Zhong Yu,[a,b] Shanshan Zhao,[a,b] Fangang Meng[a,b]

[a]School of Environmental Science and Engineering, Sun Yat-sen University, Guangzhou, People's Republic of China

[b]Guangdong Provincial Key Laboratory of Environmental Pollution Control and Remediation Technology, Guangzhou, People's Republic of China

ABSTRACT The aim of this work was to better understand the roles of extracellular polymeric substances (EPS) in membrane biofouling at the single-strain level. In the present study, a total of 23 bacterial strains were isolated from a sludge sample. The EPS extracted from pure-cultured bacteria were assessed for their fouling potentials and were simultaneously analyzed using Fourier transform infrared spectroscopy (FTIR). Further, the impact of calcium on the chemical composition of EPS and membrane fouling behavior was investigated in a strain-dependent manner. The EPS of the 23 bacterial strains exhibited different IR features for protein and polysaccharide regions. In addition, an α-1,4-glycosidic linkage (920 cm^{-1}) and amide II (1,550 cm^{-1}) correlated very well with the fouling potentials of all pure-cultured bacteria. In contrast to low-fouling strains, medium- and high-fouling strains exhibited two distinct peaks at 1,020 cm^{-1} (uronic acids) and 1,250 cm^{-1} (*O*-acetyl), which accelerate membrane fouling given their gelling capacities. In the presence of calcium, the fouling potential of a high-fouling strain (*Bacillus* sp. strain JSB10) was profoundly reduced ($P < 0.0005$) due to the binding activity of an α-1,4-glycosidic linkage and amide II with calcium. However, the impact of calcium on a low-fouling strain (*Vagococcus* sp. strain JSB21) was insignificant. Two-dimensional FTIR correlation spectroscopic (2D-FTIR-COS) analysis further revealed that the susceptibilities of functional groups to calcium largely relied on the composition and abundance of the above-described functional groups in EPS. These findings suggest that bacterial strains with different fouling potentials exhibit varied responses to calcium.

IMPORTANCE Membrane biofouling is one of the main challenges for the operation of membrane-based processes used for water and wastewater treatment. This study revealed the functional determinants of EPS in membrane biofouling of 23 bacterial strains isolated from a full-scale membrane bioreactor (MBR) plant. We found that an α-1,4-glycosidic bond, amide II, and uronic acids of EPS significantly correlated with the fouling potentials of bacteria. The roles of these EPS groups in membrane fouling were impacted by calcium resulting from EPS-calcium interactions. In addition, our results also demonstrated that any perturbations in the sludge bacterial community in MBRs can lead to varied filtration potentials of the bulk liquor.

KEYWORDS extracellular polymeric substances, functional groups, membrane fouling, membrane bioreactors, bacterial attachment

The filtration performance of membrane bioreactors (MBRs) inevitably declines with increased working time due to the deposition of biotic and abiotic materials onto membrane surfaces or into membrane pores (1). A growing body of literature has explored the mechanism involved in biofouling for the development of effective

Received 1 April 2018 **Accepted** 20 May 2018

Accepted manuscript posted online 1 June 2018

Citation Maddela NR, Zhou Z, Yu Z, Zhao S, Meng F. 2018. Functional determinants of extracellular polymeric substances in membrane biofouling: experimental evidence from pure-cultured sludge bacteria. Appl Environ Microbiol 84:e00756-18. https://doi.org/10.1128/AEM.00756-18.

Editor Shuang-Jiang Liu, Chinese Academy of Sciences

Address correspondence to Fangang Meng, mengfg@mail.sysu.edu.cn.

membrane fouling mitigation strategies (2–4). Most of the previous investigations focused on sludge characteristics or bacterial communities rather than an individual strain. This focus results in considerable uncertainty with regard to the biofouling mechanisms given the complexity of the mixed liquor of activated sludge. As such, some contradictory conclusions in the literature on biofouling have been reported (1, 5, 6). For instance, two sludge samples with the same net soluble microbial products (SMPs) can exhibit different fouling behaviors (5). Another widely explored heterogeneous material in biofouling studies is bio-cake formed on membranes. It is well known that microbial activities are not uniform in the cake layer. An oxygen-depleted environment exists in the deeper regions of bio-cake, where the microbial activity and live-to-dead-cell ratio are reduced (7) compared with levels near the bulk region. In addition, the chemical compositions might change with the increased working time (8). Thus, activated sludge and bio-cake might not be suitable choices for studying biofouling mechanisms. In fact, activated sludge and bio-cake are mainly composed of bacterial cells, which are responsible for the yield and degradation of fouling-causing biopolymers.

Extracellular polymeric substances (EPS) are one of the primary constituents in bacterial aggregates (9). An increase in bound EPS can lead to a reduction in the filterability of sludge (10), flux decline (3, 11), and increases in cake resistance (12). However, the results with respect to the roles of EPS in membrane fouling remain confusing. On the other hand, membrane fouling is highly correlated with the amount of EPS (13). In addition, some studies demonstrated that the chemical composition of EPS was more critical for fouling development (14). In recent years, model bacterial species (e.g., *Escherichia coli*, *Pseudomonas* spp., and *Staphylococcus aureus*) have been used to study biofouling behaviors (15–17). The results from these previous attempts are conflicting due to different experimental conditions or filtration modes used. Hence, it is essential to characterize the EPS of a number of pure-cultured strains from MBR sludge to provide more detailed knowledge regarding the linkage between EPS and membrane fouling.

Analysis of purified EPS from each sludge bacterial species using Fourier transform infrared spectroscopy (FTIR) helps in distinguishing the environmental isolates based on their fouling potentials (18). EPS contains charged functional groups (e.g., carboxyl and hydroxyl groups) and polar groups (e.g., aliphatics and aromatics) (19–21). These groups determine bacterial aggregation/flocculation (22, 23), fouling issues (24), and biofilm development (25) in both engineered and natural systems. For instance, the β-sheet, β-turn, and random coils of proteins in EPS are related to flocculation and deflocculation (26). EPS constituents can also adsorb heavy metals (e.g., Cr^{3+}) by forming metal-ligand complexes between carboxylic functional groups of EPS and metal ions (27). In addition, specific interactions between polysaccharides and calcium have substantial effects on membrane fouling given that Ca^{2+} can act as a good coagulant, leading to the production of coagulant flocs (28). Some reports have assessed the effect of calcium ions on EPS (cell-free) fouling propensity (12, 29), but a whole-cell approach has not been reported to date. Such attempts have great implications on the understanding of membrane fouling of activated sludge or the development of fouling control methods (30). However, the abundance of functional groups in EPS and their roles in membrane biofouling are poorly understood.

In this study, a total of 23 bacterial strains were isolated from real wastewater sludge in a full-scale MBR plant, identified by 16S rRNA gene sequence analysis, and physicochemically characterized using approaches based on cell-free EPS (i.e., dry weight, polysaccharide, and protein) and whole cells (i.e., viscosity, zeta potential, and membrane fouling potential). The membrane fouling behavior of bacterial strains was investigated using short-term filtration tests. The EPS functional groups of bacterial strains were characterized by FTIR to link functional groups with their fouling propensity. Moreover, the impact of calcium on the filtration performance of the bacterial strains was investigated, and the interactions of EPS functional groups with calcium were revealed by two-dimensional correlation spectroscopic (2D-COS) analysis.

RESULTS

Strain properties and identification. A total of 23 bacterial strains (named JSB1 to JSB23) were isolated from the sludge sample. Of these strains, 10 strains were Gram positive, and the remaining strains were Gram negative. The characteristics of these bacteria are listed in Table 1, and their microscopic photos based on Gram staining are presented in Fig. S1 in the supplemental material. Most of these bacteria were rod shaped, with dimensions of 0.6 to 1.6 by 1.1 to 4.7 μm. The majority of the strains produced white colonies (LB agar) and reached stationary phase within 24 h (LB broth) (as listed in Table S1). According to a BLASTn search of 16S rRNA gene sequences (1,375 bp), 99 to 100% identity was noted within the existing identified DNA sequence database. Nine strains belonged to the genus *Bacillus*; 4 strains were *Aeromonas*; 3 strains were *Klebsiella*; one strain each was from the genera *Paenochrobactrum*, *Proteus*, *Serratia*, and *Vagococcus*; and three strains were unidentified. The EPS layer tightly bound to the bacteria was observed under a light microscope after capsule staining (Fig. S2). The bound EPS dry weight of these strains was in the range of 0.58 to 1.28 g/liter. The protein-to-polysaccharide ratios in the EPS of all 23 sludge bacteria were $<$1.0, because the concentration of protein (5.2 to 53.0 mg/liter) was reduced compared with that of polysaccharides (52 to 530 mg/liter). Apparent viscosities of these cell suspensions were observed in the range of 1.92 to 2.37 mPa/s, whereas that of the control sample (0.9% NaCl solution) was 1.91 mPa/s (at a shear rate of 122.5 s^{-1}). When the shear rate increased from 122.5 to 244.9 s^{-1}, the viscosities of most strains (19 out of 23 strains) increased by 24 to 59% (as shown in Table S2). The zeta potential of bacteria (intact bound EPS) ranged from -1.61 to -17.40 mV.

FTIR spectra of bound EPS of pure-cultured strains. The FTIR spectra of bound EPS of the individual bacterial strains are presented in Fig. 1, and the relevant characteristic functional groups are listed in Table S3. All the absorbance bands are typical characteristic peaks of bacteria reported elsewhere (31). Specifically, two peaks at 1,640 cm^{-1} and 1,550 cm^{-1} in the spectra of most strains were attributed to the presence of the amide I and amide II groups, respectively (32). A peak at 1,400 cm^{-1} was assigned to symmetric stretching of the $-COO^-$ group associated with amino acids in the following samples: *Serratia* sp. strain JSB1, *Bacillus* sp. strains JSB10 and JSB11, *Bacillus* sp. strain JSB13, *Bacillus* sp. strains JSB17 and JSB19, and *Proteus* sp. strain JSB20 (20, 33). A strong peak at ~1,100 cm^{-1} was attributed to the presence of polysaccharides (20) and was identified in all samples. The presence of uronic acid was indicated by a peak at ~1,020 cm^{-1} (34), which was only detected in the EPS from *Bacillus* sp. JSB10, *Klebsiella* sp. strain JSB15, *Klebsiella* sp. strain JSB16, and *Klebsiella* sp. strain JSB18. In addition, a shoulder peak at 920 cm^{-1} was detected in the EPS of *Bacillus* sp. JSB10, *Klebsiella* sp. JSB15, *Klebsiella* sp. JSB16, *Klebsiella* sp. JSB18, and *Proteus* sp. JSB20. This peak is attributed to the presence of an α-1,4-glycosidic bond. Taken together, the FTIR spectra predominantly indicated 3 functional groups associated with each region of proteins (1,400, 1,550, and 1,640 cm^{-1}) and polysaccharides (920, 1,020, and 1,100 cm^{-1}) in EPS.

According to the characteristic IR features (regions I and II) in polysaccharide and protein regions, FTIR spectra of the 23 strains were divided into 4 groups (Fig. 1a to d), as follows: (i) 15 strains did not exhibit either region I or region II (Fig. 1a), (ii) 3 strains exhibited region I (Fig. 1b) and belonged to the genus *Klebsiella*, (iii) 3 strains exhibited region II and belonged to the genus *Aeromonas* (Fig. 1c), and (iv) only one strain (i.e., *Bacillus* sp. JSB10) exhibited both regions I and II (Fig. 1d). These results imply the genus-dependent nature of the EPS structure to a certain extent. Considering the potential overlapping of important peaks at 900 to 960 cm^{-1} and 1,500 to 1,700 cm^{-1}, curve fitting was conducted, and the deconvoluted spectra are presented in Fig. 2. The results showed that α-1,4-glycosidic bond (~920 cm^{-1}), amide I (1,600 to 1,700 cm^{-1}), and amide II (1,500 to 1,600 cm^{-1}) peaks were exactly extracted from the FTIR spectra. Specifically, the IR absorbance intensity of the α-1,4-glycosidic bond for the EPS of *Vagococcus* sp. JSB21, *Proteus* sp. JSB20, and *Bacillus* sp. JSB10 were 0.05 (Fig. 2b), 0.12

TABLE 1 Characteristics of pure cultures of sludge bacteria isolated from a full-scale MBR

Sl. no.	Isolate	Identification by 16S rRNA gene sequence (% homology)	Gram stain[a]	Shape[b]	Size (μm)[c]	Wt or concn from incubation for 48 h in glucose-yeast extract broth			Protein/polysaccharide ratio	Viscosity (mPa/s)	Zeta potential (mV)
						EPS dry wt (g/liter)	Protein (mg/liter)	Polysaccharide (mg/liter)			
1	JSB1	*Serratia* sp. (100)	N	R	1.9 by 0.7	1.28 ± 0.77	43.6	249	0.17	1.94	−9.14
2	JSB2	*Bacillus* sp. (99)	P	R	4.1 by 1.6	0.81 ± 0.04	12.4	111	0.11	1.96	−5.32
3	JSB3	*Bacillus* sp. (100)	P	R	2.2 by 0.8	0.83 ± 0.10	12.2	146	0.08	2.02	−11.00
4	JSB4	*Aeromonas* sp. (100)	N	R	2.1 by 0.8	1.13 ± 0.65	38.0	255	0.15	1.98	−15.30
5	JSB6	*Bacillus* sp. (100)	P	R	2.7 by 0.8	1.10 ± 0.24	10.2	192	0.05	2.37	−13.80
6	JSB7	*Bacillus* sp. (99)	P	R	3.6 by 1.1	0.87 ± 0.02	53.0	227	0.24	2.00	−6.72
7	JSB8	*Aeromonas* sp. (100)	N	R	1.6 by 0.6	0.67 ± 0.14	28.0	77	0.37	1.92	−1.85
8	JSB9	*Aeromonas* sp. (100)	N	R	3.0 by 0.9	0.58 ± 0.12	10.6	159	0.68	1.99	−3.26
9	JSB10	*Bacillus* sp. (99)	P	R	2.0 by 1.3	0.89 ± 0.11	30.6	290	0.1	1.96	−4.23
10	JSB12	*Aeromonas* sp. (99)	N	R	1.8 by 0.8	0.69 ± 0.03	10.2	199	0.05	1.98	−1.61
11	JSB13	*Bacillus* sp. (100)	P	R	3.1 by 1.1	0.86 ± 0.07	21.2	190	0.11	2.00	−4.75
12	JSB14	*Bacillus* sp. (100)	P	R	3.7 by 1.1	0.93 ± 0.22	34.6	530	0.06	1.96	−9.10
13	JSB15	*Klebsiella* sp. (100)	N	R	1.6 by 0.8	1.27 ± 0.25	21.4	269	0.08	2.08	−9.47
14	JSB16	*Klebsiella* sp. (100)	N	R	1.5 by 1.0	0.96 ± 0.43	14.0	72	0.2	2.09	−15.90
15	JSB17	*Bacillus* sp. (100)	P	R	2.7 by 1.1	0.83 ± 0.00	35.6	234	0.15	2.03	−6.64
16	JSB18	*Klebsiella* sp. (100)	N	R	1.1 by 0.8	1.12 ± 0.15	8.2	52	0.16	2.01	−15.60
17	JSB20	*Proteus vulgaris* (99)	N	R	1.2 by 0.7	0.81 ± 0.26	37.4	151	0.24	1.97	−8.24
18	JSB21	*Vagococcus* sp. (99)	P	C	0.8	0.60 ± 0.08	12.8	190	0.07	2.01	−15.50
19	JSB22	*Bacillus* sp. (99)	P	R	1.8 by 1.3	0.83 ± 0.11	19.2	194	0.1	2.02	−12.00
20	JSB23	*Paenochrobactrum* sp. (100)	N	R	1.8 by 0.7	0.64 ± 0.03	9.8	133	0.07	1.89	−17.40
21	JSB5	Unidentified bacterium	N	R	4.7 by 0.8	1.26 ± 0.60	5.2	281	0.02	1.99	−1.71
22	JSB11	Unidentified bacterium	N	R	1.9 by 0.8	0.73 ± 0.11	6.0	121	0.05	2.01	−12.10
23	JSB19	Unidentified bacterium	P	C	3.7	0.83 ± 0.25	21.8	494	0.04	2.02	−17.20

[a]N, negative; P, positive.

[b]R, rod; C, coccus.

[c]Single values represent the cell diameter.

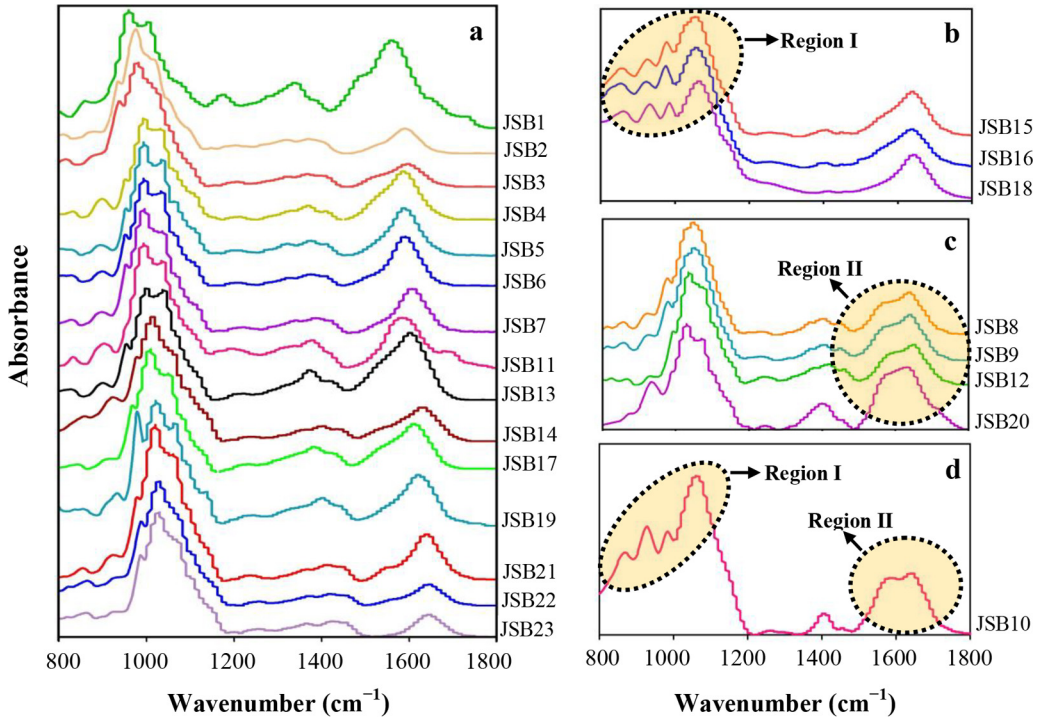

FIG 1 Fourier transform infrared spectroscopic analysis of bound EPS of different pure-culture bacteria. Grouping is based on structural differences in the FTIR spectra among different bacteria. (a) FTIR spectra without a high absorbance region for polysaccharides (region I) and proteins (region II). (b to d) FTIR spectra of region I (b), region II (c), and regions I and II (d).

(Fig. 2e), and 0.18 (Fig. 2h), respectively. Interestingly, the IR absorbance intensity of amide II varied significantly for these three strains, at 0.0599 (Fig. 2c), 0.23 (Fig. 2f), and 0.264 (Fig. 2i), respectively. In contrast, the absorbance intensity of the amide I bond did not significantly differ among the three selected strains.

Fouling potentials of pure-cultured strains. The flux decline curves of 23 strains are presented in Fig. S3, and 3 representative curves are presented in Fig. 3a. The relevant unified membrane fouling index (UMFI) values of these 23 strains were calculated, and the results are presented in Fig. 3b. According to the UMFI values, the strains were divided into 3 groups, low-, medium-, and high-fouling-causing bacteria, with UMFI values of $<$0.1, 0.1 to 0.2, and $>$0.2, respectively. The flux of the high-fouling strain (*Bacillus* sp. JSB10) quickly decreased, whereas the flux of the low-fouling strain (e.g., *Vagococcus* sp. JSB21) decreased slowly. The lowest (*Bacillus* sp. JSB17; UMFI, 0.054) and highest (*Bacillus* sp. JSB10; UMFI, 0.404) UMFI values within the same genus of *Bacillus* offered overwhelming evidence of the strain-dependent nature of fouling behavior. Similar findings are presented in the literature (35). Specifically, 5 strains of *Bacillaceae* isolated from fouled membrane exhibited significantly different fouling behaviors. According to the correlation analysis (Table S4), only the IR absorbance intensity of the α-1,4-glycosidic bond (P*r* [Pearson correlation coefficient *r*] = 0.6672; $P < 0.0005$) and amide II (P*r* = 0.5957; $P < 0.005$) correlated well with the UMFI (as shown in Fig. 4a and b). These findings indicate that the α-1,4-glycosidic bond or amide II may play a key role in membrane fouling potentials during the filtration of these pure-culture cells.

Ca-mediated fouling propensity of pure-cultured bacteria. The presence of divalent cations and ionic strength mediates EPS properties and fouling behavior. In Fig. 5, the responses of these three bacterial strains varied. For the high-fouling strain *Bacillus* sp. JSB10, the presence of calcium ions led to a significant decrease in fouling propensity, and the UMFI was reduced from 0.38 to 0.1135 ($P < 0.0005$) (Fig. 5a). This result suggests that the presence of divalent cations might aid in mitigating the fouling

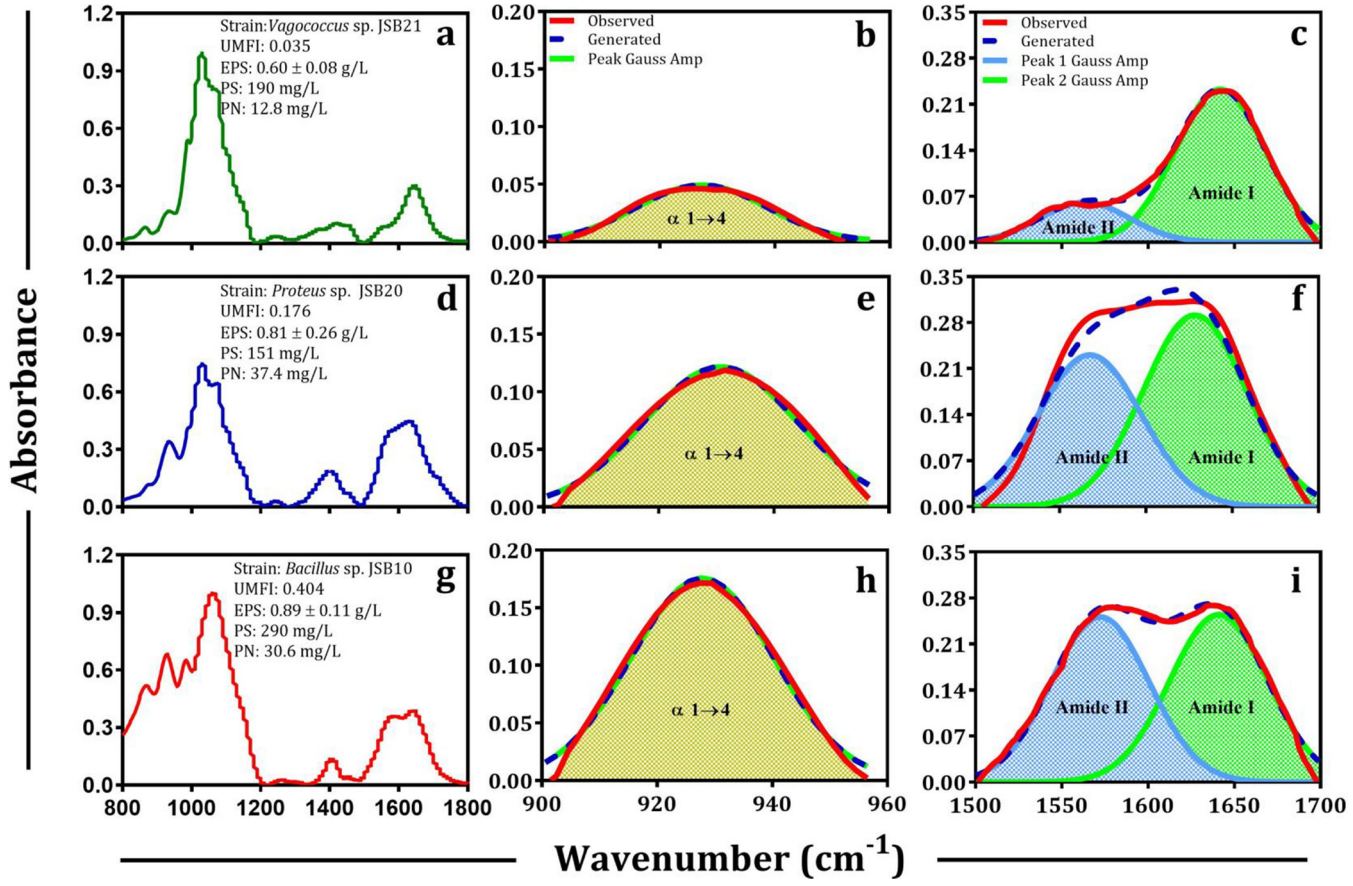

FIG 2 FTIR spectra of bound EPS of low-fouling (a), medium-fouling (d), and high-fouling (g) bacteria are shown. Second derivative revolution enhancement and curve-fitted (r^2 0.999, interactions [number of iterations in the fitting] = 7) polysaccharide (b, e, and h) and protein (c, f, and i) region of bound EPS of respective strains are shown. The curve-fitted spectra (r^2 0.99 to 0.999, interactions = 7) were obtained by the Fourier deconvolution of Gaussian instrument response function, followed by application of the AutoFit Peaks II second derivative function for the polysaccharide region (b, e, and h), and the AutoFit Peaks III deconvolution function for protein regions (c, f, and i). UMFI, unified membrane fouling index; PS, EPS-polysaccharide; PN, EPS-protein.

potential of this type of bacterial strain. The presence of a lower calcium concentration (0.1 mM) with identical ionic strength resulted in a lower UMFI than that noted with 0.5 mM calcium. This phenomenon is similar to that reported in a previous study demonstrating that a low calcium concentration resulted in gel formation of alginate on membranes, whereas a high calcium concentration led to gel breakage (36). As observed in Fig. 5b, the particle size of *Bacillus* sp. JSB10 bacteria was not significantly influenced by Ca^{2+}, implying that this high-fouling strain might not exhibit aggregation in the presence of Ca^{2+}. Thus, the mitigated fouling of *Bacillus* sp. JSB10 bacteria in the presence of Ca^{2+} was likely due to the modification of the conformation of EPS molecules or the shielding effects on some EPS functional groups (37). However, for the medium-fouling strain case (*Proteus* sp. JSB20), the presence of 0.5 mM Ca^{2+} increased the UMFI from 0.1685 (without Ca^{2+} dosage) to 0.2240. The presence of calcium ions may enhance the adsorption of polysaccharides or proteins on membranes for this type of strain (12, 38). Regarding the low-fouling strain (*Vagococcus* sp. JSB21), the addition of Ca^{2+} did not affect the UMFI, as shown in Fig. 5a. A recent investigation also reported ambivalent roles of Ca^{2+} in EPS properties and membrane fouling of two bacterial strains, i.e., the presence of Ca^{2+} increased the adsorption ability of the wild-type strain of *Pseudomonas aeruginosa* PAO1 but decreased that of the Δ*psl* mutant of PAO1 with a lower EPS content (39). To summarize, our results together with the previous findings (39) imply that the impacts of Ca^{2+} on fouling behavior of bacterial strains are highly dependent on the concentration of Ca^{2+} and functional groups of bound EPS.

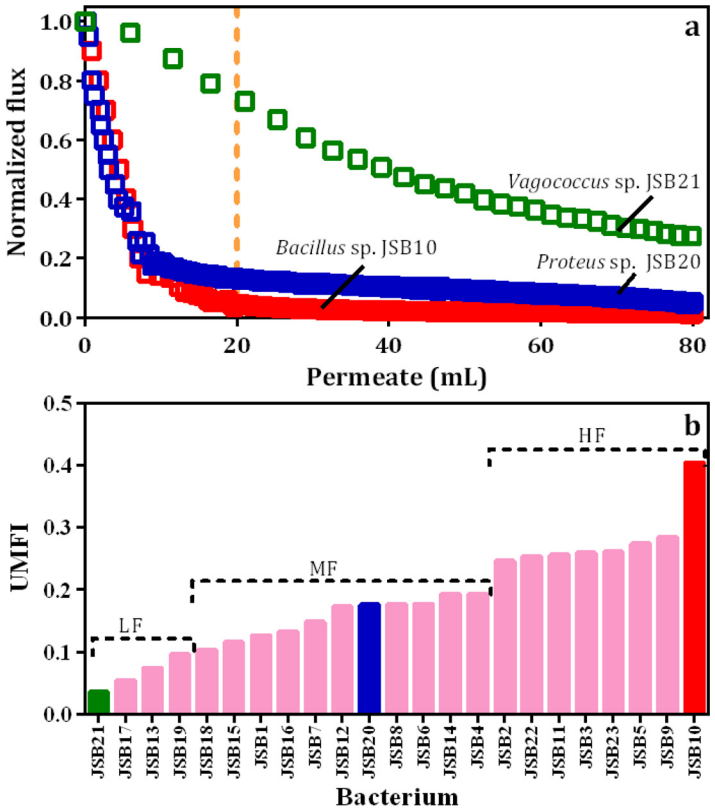

FIG 3 Values of normalized flux of selected bacterial strains (a) and unified membrane fouling index of various pure-culture bacteria (b). Dotted vertical line (a) indicates flux decline (%) by 20 ml of permeate, and values for *Vagococcus* sp. JSB21 (green), *Proteus vulgaris* JSB20 (blue), and *Bacillus* sp. JSB10 (red) were 27, 87, and 96%, respectively. Grouping in panel b was based on fouling potential. LF, low-fouling bacteria (UMFI, <0.1); MF, medium-fouling bacteria (UMFI, 0.1 to 0.2); HF, high-fouling bacteria (UMFI, >0.2).

Interactions of functional groups of EPS with Ca. To investigate the mechanism for Ca-mediated membrane fouling of these bacteria during membrane filtration, the IR spectra of EPS with addition of various concentrations of Ca^{2+} (0 to 1.0 mM) were measured. The presence of Ca^{2+} obviously changed the IR spectra of the EPS samples, including peak shape and intensity (Fig. 6). These results indicate that the functional groups of EPS could interact with Ca^{2+}, and this interaction largely depended on the Ca^{2+} concentration and type of bacterial strains. For instance, the IR peak at 1,100 cm^{-1} of the low-fouling strain (*Vagococcus* sp. JSB21) did not change significantly as the Ca^{2+} dosage changed (Fig. 6c). However, the α-1,4-glycosidic bond at 920 cm^{-1} of the high-fouling strain (*Bacillus* sp. JSB10) was strongly affected by Ca^{2+} even at a very low concentration (0.1 mM) (Fig. 6a). According to the AutoFit Peaks II second derivative function, changes in the IR absorbance intensities of six specific functional groups of EPS as a function of Ca^{2+} dosage are presented in Fig. 7. A low dosage of Ca^{2+} (0.1 mM) led to a sharp decrease in the IR absorbance of α-1,4-glycosidic bond (Fig. 7a), uronic acids (Fig. 7c), and amide II (Fig. 7f) in EPS of *Bacillus* sp. JSB10. This finding is consistent with the substantially decreased membrane fouling (i.e., UMFI values) of *Bacillus* sp. JSB10 upon the addition of Ca^{2+} (Fig. 5a). In contrast, with respect to the EPS extracted from *Vagococcus* sp. JSB21 (a low-fouling strain), the lower dosage of Ca^{2+} (0.1 to 0.3 mM) did not result in a significant decrease in the IR absorbance of the α-1,4-glycosidic bond at 920 cm^{-1} (Fig. 7m), uronic acids (Fig. 7n), and amide II (Fig. 7r). This result explains why the fouling behavior of *Vagococcus* sp. JSB21 did not respond significantly to the addition of Ca^{2+} (Fig. 5a). The IR absorbances of five functional groups in the EPS extracted from *Proteus* sp. JSB20 (a medium-fouling strain) decreased significantly in

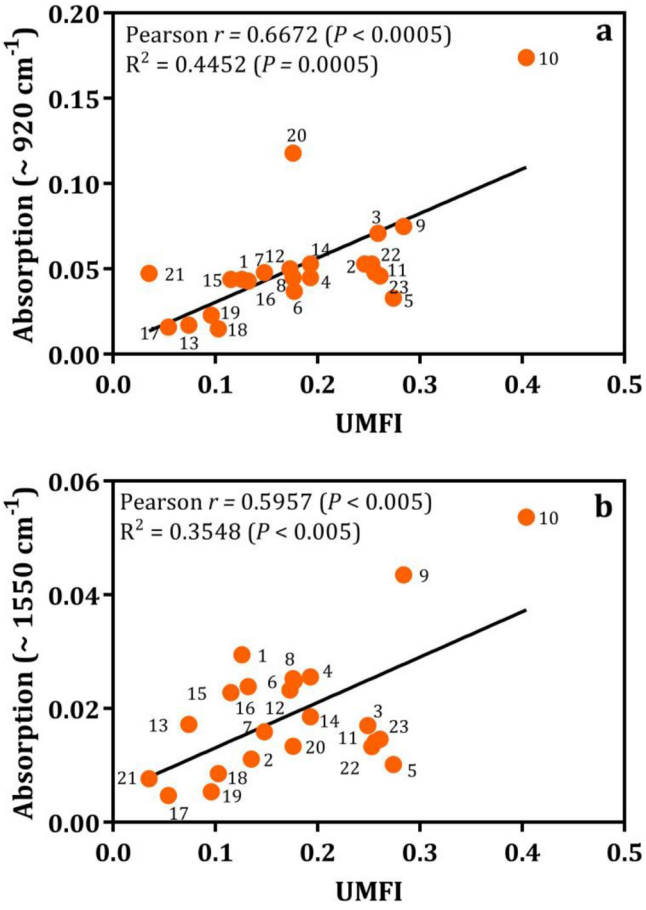

FIG 4 Correlation (fit line with linear regression) between membrane fouling potentials (UMFI) of bacteria and α-1,4-glycosidic bond (a) and amide II (-N-H) (b). Assumed data were sampled from the Gaussian population (Pearson) for correlation analysis. Absorbance values on the *y* axis were obtained from FTIR curve-fitted spectra (Fourier deconvolution of Gaussian instrument response and AutoFit Peaks II second derivative functions were applied, r^2 = 0.73 to 0.99, interactions = 7). *P* values (one-tailed) at 95% confidence interval are reported. Numerals (labeled with color circles) 1 to 23 indicate the respective strains JSB1 to JSB23. Functional groups at ~920 cm^{-1} and ~1,550 cm^{-1} are attributed to an α-1,4-glycosidic bond (66) and amide II (63), respectively.

the presence of Ca^{2+} (Fig. 7g, h, and j to l). This finding was in contrast to the increased fouling of this strain by Ca^{2+} (Fig. 5b). It was hypothesized that the membrane filtration was probably dominated by other fouling factors (i.e., substantial increases in the aggregate size of the bacteria) rather than the EPS functional groups.

Some IR peaks (e.g., 1,550 and 1,640 cm^{-1}) responded significantly even at a low Ca^{2+} dosage, whereas some IR peaks only changed at a high Ca^{2+} dosage. Thus, 2D-FTIR-COS analysis was further performed to investigate the sequential order of Ca^{2+} binding for these functional groups. In 2D-COS analysis, synchronous maps displayed autopeaks (at a diagonal position) for each bacterium (Fig. 8a, c, and e). Note that the intensities of the autopeaks represent the overall susceptibility of the corresponding structure to external perturbation. Increased intensities of autopeaks in both polysaccharide and protein regions were observed for *Bacillus* sp. JSB10 (Fig. 8a), whereas these intensities were gradually reduced in *Proteus* sp. JSB20 (Fig. 8c) and *Vagococcus* sp. JSB21 (Fig. 8e). Furthermore, an increased number of positive cross-peaks was observed (Table S5) as the fouling potentials increased. For example, *Bacillus* sp. JSB10, *Proteus* sp. JSB20, and *Vagococcus* sp. JSB21 exhibited 5, 10, and 11 peaks in their synchronous maps, respectively. Positive cross-peaks indicated that these peaks had the same response to the addition of Ca^{2+}. In contrast, negative cross-peaks in synchronous maps suggest the change in peak directions. Such peaks were only observed in *Bacillus* sp. JSB10 (10 peaks) and *Vagococcus* sp. JSB21 (4

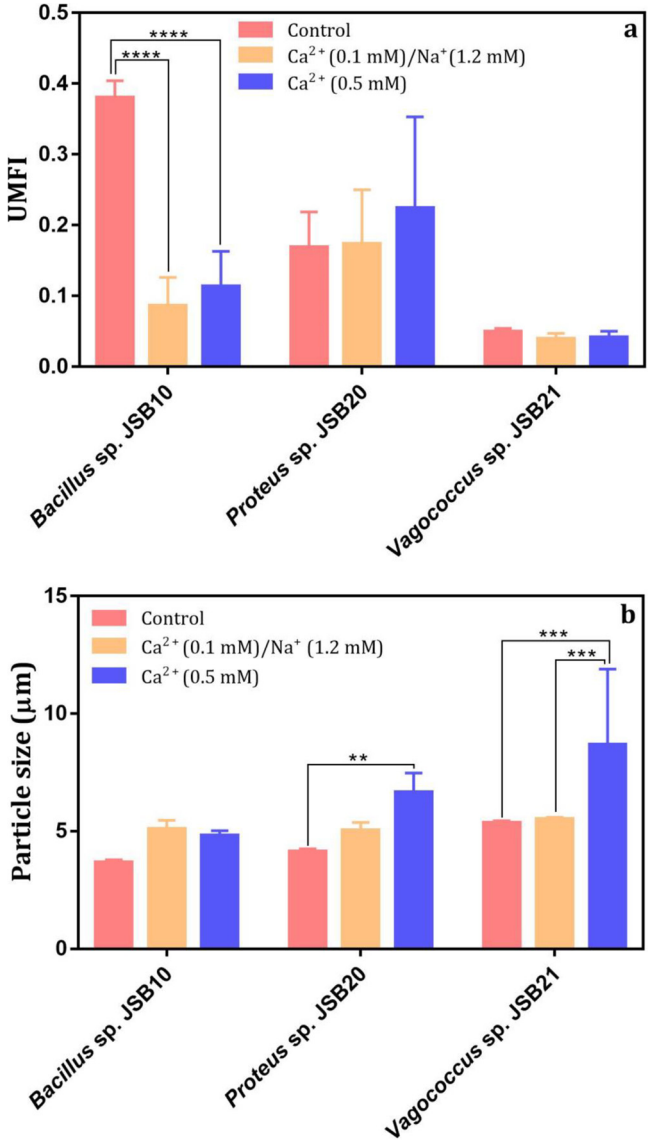

FIG 5 Effect of Ca^{2+} concentrations on membrane fouling potentials ($n = 3$) (a) and particle size ($n = 5$) (b) of selected bacterial species. The control contains respective cells in 0.9% NaCl solution of ionic strength similar to that of Ca^{2+}-amended samples. Two-way ANOVA Tukey's multiple-comparison test was performed, and adjusted *P* values (one tailed) at 95% confidence interval are reported (**, $P < 0.005$; ***, $P < 0.0005$; ****, $P < 0.00005$).

peaks), not in *Proteus* sp. JSB20 (Table S5). Asynchronous maps can reveal the sequential order of the EPS-specific structural response to perturbation by comparing the signs of cross-peaks between synchronous and asynchronous maps. As shown in Fig. 8, 12, 13, and 9 cross-peaks were detected above the diagonal line for EPS binding with Ca^{2+} in *Bacillus* sp. JSB10 (Fig. 8b), *Proteus* sp. JSB20 (Fig. 8d), and *Vagococcus* sp. JSB21 (Fig. 8f), respectively. The signs of the aforementioned cross-peaks are presented in Table S5. In summary, the changes in EPS functional groups in response to Ca^{2+} exhibit the following order (Table S5): (i) α-1,4-glycosidic bond (920 cm^{-1}) > uronic acids (1,020 cm^{-1}) > 1,100 cm^{-1} > amide I (1,640 cm^{-1}) > amide II (1,550 cm^{-1}) > C═O (1,400 cm^{-1}) for *Bacillus* sp. JSB10; (ii) amide II > uronic acids > C═O > α-1,4-glycosidic bond > amide I for *Proteus* sp. JSB20; and (iii) 1,100 > C═O > amide I > amide II > uronic acids > α-1,4-glycosidic bond for *Vagococcus* sp. JSB21. This finding suggests that the susceptibilities of the functional groups of different bacteria to Ca^{2+} differed and likely depended on their

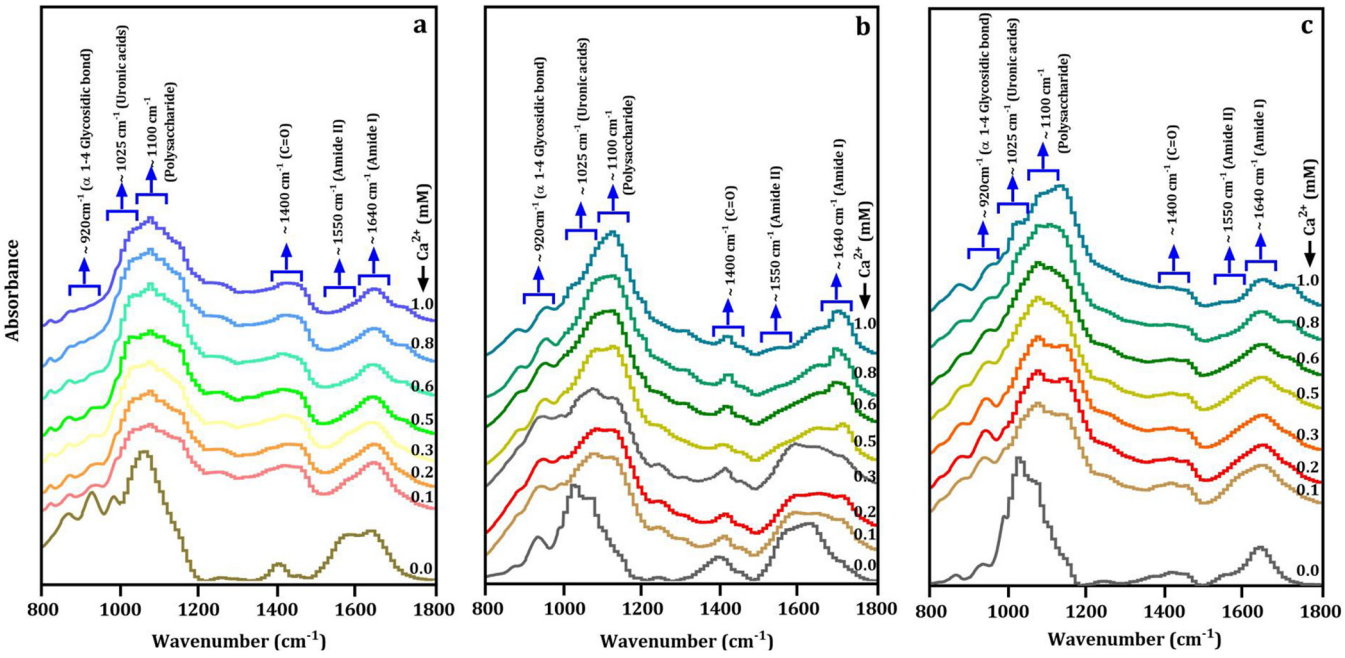

FIG 6 FTIR spectra of EPS-Ca^{2+} complexes of high-fouling (*Bacillus* sp. JSB10) (a), medium-fouling (*Proteus* sp. JSB20) (b), and low-fouling (*Vagococcus* sp. JSB21) (c) bacteria. Functional groups of EPSs are shown as influenced by different concentrations of calcium from 0 to 1.0 mM.

abundance in an EPS matrix. Overall, 2D-FTIR-COS analysis findings provide new insights into the different responses of UMFI to Ca^{2+} in the three bacterial strains.

DISCUSSION

Bacterial strain-specific features of IR spectra of EPS. During membrane-based processes for water and wastewater treatment, membrane fouling inevitably occurs due to the gelling nature or viscosity of EPS, which generally involves a network of cross-linked polysaccharide chains (40). In addition, proteins also contribute to membrane fouling as a result of their hydrophobic interactions with membranes or other foulants. Previously, researchers focused on the characterization of EPS and SMPs in the mixed liquor of suspended sludge composed of various bacteria. Given the complex nature of such a sludge bacterial community, the reported results differed or were even contradictory. In this work, our primary objective is to understand the EPS composition and roles in membrane biofouling at a single-strain level. Our FTIR analysis demonstrated that the EPS of each strain exhibited unique IR features. For instance, the EPS of *Bacillus* sp. JSB10 contained IR bands in both region I (920, 1,020, and 1,100 cm^{-1}) and region II (1,550 and 1,640 cm^{-1}), which generally differed from other *Bacillus* strains (e.g., JSB2, JSB3, JSB6, and JSB7). In addition, three strains belonging to the genus *Klebsiella* also showed strong IR bands in region I. Evidently, the presence of region I, i.e., the simultaneous presence of three peaks at 920, 1,020, and 1,100 cm^{-1}, is attributed to glycogen (41). Of note, these three peaks in combination with a peak at 1,250 cm^{-1} is indicative of alginate-like polysaccharides (42), e.g., the EPS from *Bacillus* sp. JSB10 and *Proteus* sp. JSB20. Differences in the quantities and compositions of EPS among the strains are likely attributed to differing metabolic activities (43) or varied DNA compositions. For example, significant differences in EPS between parent and mutant strains have been reported in numerous studies (42, 44, 45) and support our conclusion of the strain-specific IR features of EPS. Moreover, glucose-yeast extract medium and the steady-growth stage of bacteria (48 h) were used for EPS formation and extraction in this work. Apparently, the culture medium and incubation time could also have a great impact on the characteristics and composition of bacterial EPS. In the future, the effects of different culture media and growth phases on EPS production and

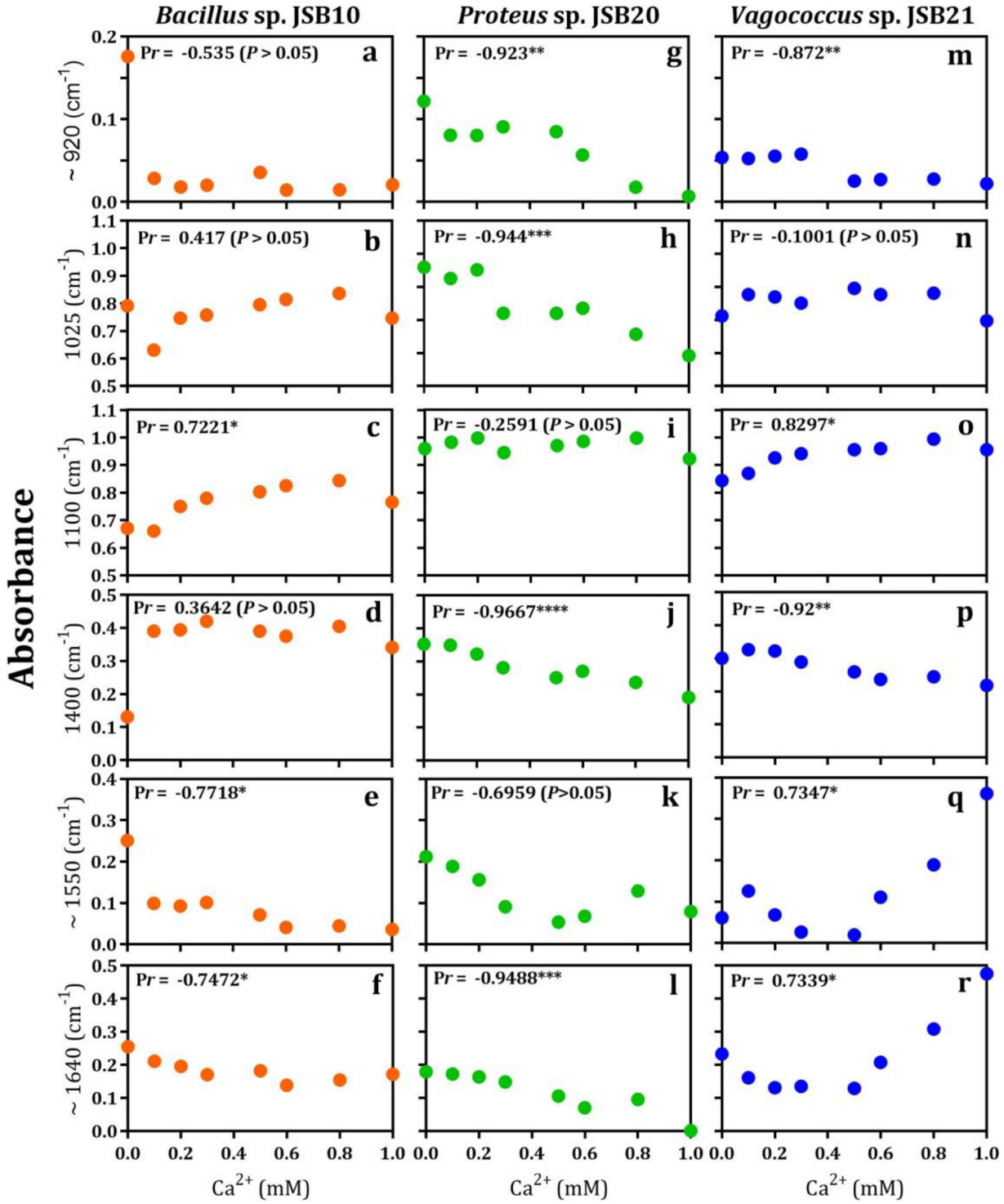

FIG 7 Changes in the absorbance of FTIR spectra of functional groups of EPS-Ca^{2+} complexes of monospecies cultures: high-fouling (*Bacillus* sp. JSB10) (a to f), medium-fouling (*Proteus* sp. JSB20) (g to l), and low-fouling (*Vagococcus* sp. JSB21) (m to r) bacteria. The curve-fitted spectra (r^2, 0.99 to 0.999, interactions = 7) were obtained by Fourier deconvolution of Gaussian instrument response function, followed by the application of AutoFit Peaks II second derivative function for an α-1,4-glycosidic bond and AutoFit Peaks III deconvolution function for amide I and amide II functional groups. *P* values (one-tailed) at a 95% confidence interval were as follows: *, $P < 0.05$; **, $P < 0.005$; ***, $P < 0.0005$; ****, $P < 0.0001$.

bacterial properties and the association of these factors with membrane fouling behaviors should be clarified.

Functional determinants of EPS in membrane biofouling. In previous studies, membrane fouling was generally attributed to the presence of some typical IR

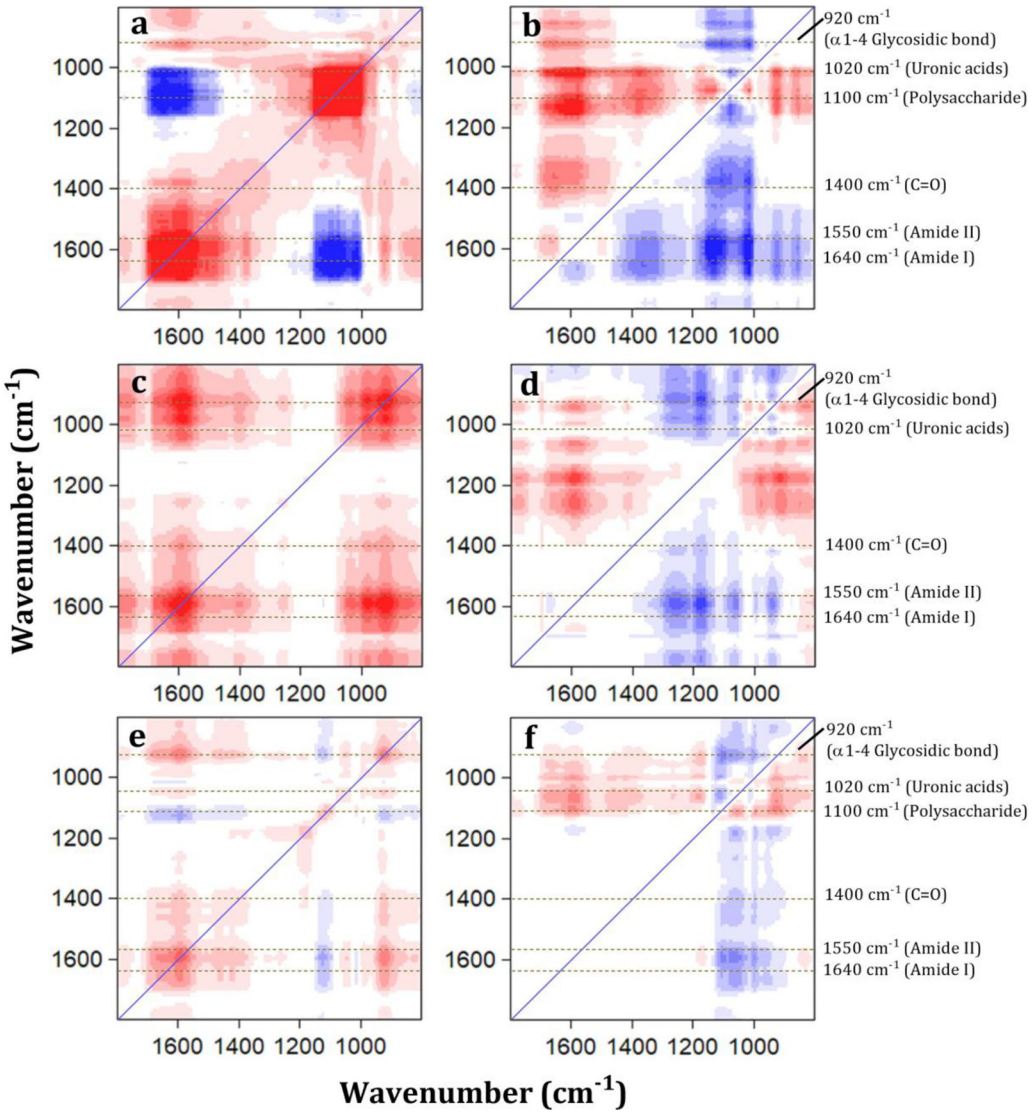

FIG 8 Two-dimensional correlation maps (synchronous and asynchronous) generated from the 800 to 1,800 cm^{-1} region of the FTIR spectra of EPS-Ca^{2+} complexes of high-fouling (*Bacillus* sp. JSB10) (a and b), medium-fouling (*Proteus* sp. JSB20) (c and d), and low-fouling (*Vagococcus* sp. JSB21) (e and f) bacteria. The concentration of calcium used was in the range of 0 to 1.0 mM. Red and blue represent positive and negative correlations, respectively. A greater color intensity indicates a stronger correlation, and a weaker color intensity indicates a weaker correlation.

bands (24), such as the broad peak at 1,100 cm^{-1} and two protein peaks at 1,640 and 1,550 cm^{-1}. However, some unique IR features, including peaks at 920 and 1,020 cm^{-1}, have not been given sufficient attention likely due to the complex composition of the analyzed samples, such as activated sludge and bio-cake. Based on the IR analysis of the EPS extracted from 23 strains, three IR peaks were associated with polysaccharides (920, 1,020, and 1,100 cm^{-1}), and three peaks were associated with proteins (1,400, 1,550, and 1,640 cm^{-1}). Statistical analysis revealed that the presence of an α-1,4-glycosidic bond (920 cm^{-1}) and amide II (1,550 cm^{-1}) were highly significant ($P < 0.005$ or <0.0005) for UMFI values. In comparison, the broad peak at 1,100 cm^{-1}, which has been previously considered to be an important indicator of membrane fouling, did not correlate well ($Pr = -0.2363$; $P > 0.05$) with UMFI values (Table S3). In addition, α-1,4-glycosidic linkages are often present in sugars or polysaccharides (e.g., maltose and maltotetrose) with high gelling properties given their role of binding long-chain monosaccharide units into a polymeric carbohydrate molecule (46). In contrast, β-1,4-glycosidic linkages are

normally present in cellulose. As previously mentioned, the gelling nature of polysaccharides can greatly enhance the deposition of bacteria, particularly when the membrane filtration system is operated at a high pressure. In addition, uronic acids (1,020 cm^{-1}) and *O*-acetyl groups (1,250 cm^{-1}) can indicate the presence of alginate-like polysaccharides (42), which also exhibit a strong gelling property (36). Okamura et al. documented that the fouling potential of polysaccharides increased linearly as uronic acid levels increased (47). Nivens et al. found that the *algJ* mutant strain of *Pseudomonas aeruginosa* that yielded alginate lacking *O*-acetyl groups exhibited a 5-fold reduced ability to form biofilm compared with its parent (48). Given that the two bands (1,020 and 1,250 cm^{-1}) were only detected in a few strains, such as *Bacillus* sp. JSB10 and *Proteus* sp. JSB20, no correlation was identified between these two bands and the UMFI values (Table S3). Further studies should be conducted to confirm the roles and significance of these functional units (uronic acids and *O*-acetylation) in membrane biofouling development.

Similarly, amide II was often detected in the EPS of high- or medium-fouling strains, and this IR peak correlated well ($Pr = 0.5957$; $P < 0.005$) with UMFI values. In fact, the IR absorbance of amide II has been used as a marker for determining the biofilm biomass formed by *Pseudomonas aeruginosa* (48) and *Pseudomonas fluorescens* (49). Amide I significantly contributes to cell-cell interactions, such as bacterial aggregation/flocculation (22, 23) or bacterial attachment (50). The presence of large amounts of hydrophobic amino acids and a high level of proteins with a loose structure in EPS greatly enhanced the aggregation ability of sludge (23). Nevertheless, amide I was present in almost all pure-cultured strains in our current study, and no differences were noted among the IR absorbances of amide I. Thus, amide I cannot be used as a marker to distinguish the fouling propensities of various bacterial strains or communities. Further investigations are also recommended to reveal the fouling mechanisms of these specific functional groups (α-1,4-glycosidic linkages, uronic acids, *O*-acetyl groups, amide I, and amide II) using well-defined mixed cultures or mutants of some interesting strains.

Roles of EPS-cation interactions in membrane biofouling. EPS plays a significant role in the attachment of bacterial cells to the surface due to the contribution of charged functional groups (e.g., carboxyl, hydroxyl, phenolic, phosphoric, and sulfhydryl groups) and polar groups (e.g., aliphatics and aromatics in proteins and hydrophobic regions in carbohydrates) in EPS (19). EPS compounds readily interact with divalent cations (e.g., Ca^{2+} and Mg^{2+}) and form complexes in the presence of these functional groups. On one hand, divalent cations neutralize the negative charges carried by EPS molecules (51). On the other hand, divalent cations aid in macromolecule assembly resulting from the ion bridging role of divalent cations. The formation of EPS-Ca^{2+} complexes can enhance the aggregation of inorganic colloids in natural water as a result of gel-like bridging (52). In our study, we also noted an increased aggregate size for *Proteus* sp. JSB20 in the presence of Ca^{2+} (Fig. 5b). A number of studies have also demonstrated that Ca^{2+} can enhance fouling of natural organic matter or EPS (12, 53), thus leading to a requirement of more intensive chemical cleaning (53). However, our current study implies that some bacteria or EPS may not follow such a role, i.e., the presence of Ca^{2+} did not result in changes in the fouling propensities of some bacterial strains (*Vagococcus* sp. JSB21) (Fig. 5a). Determining the binding capacity of a given functional group on divalent cations using well-defined tests or more specific strains is of significant interest. The results from 2D-FTIR-COS analysis in our study suggest that the binding capability of a given functional group relies on its chemical structure and relative abundance in EPS.

In conclusion, this study demonstrated that (i) the IR spectra of the pure-cultured bacteria overall occurred a strain-dependent manner; (ii) α-1,4-glycosidic linkage (920 cm^{-1}), amide II (1,550 cm^{-1}), and uronic acids (1,020 cm^{-1}) were essential for the fouling potentials of bacterial strains; (iii) the presence of calcium changed the fouling potentials of bacterial strains; and (iv) the susceptibility of functional groups in EPS to

calcium depended on EPS functional group composition and abundance. The genus and strain dependence of EPS composition together with fouling behavior can explain why confusing or contradictory results are often reported in the literature, given that any change in the bacterial community, even at the strain level, can lead to a profound alteration of EPS composition. In the near future, further studies are required to determine the roles of uronic acids and *O*-acetylation in biofilm formation on membranes. In addition, the fouling behavior of mixed cultures should be explored by focusing on the interaction of EPS from various strains.

MATERIALS AND METHODS

Isolation and identification of bacterial strains. Bacterial strains were isolated from a sludge sample collected (31 May 2016) from a local full-scale MBR plant (Jingxi municipal wastewater treatment plant, Guangzhou, People's Republic of China). This plant is an underground wastewater treatment plant (WWTP) occupying 1.8 ha, with a treatment capacity of 100,000 m^3 wastewater per day (Table S6). To isolate bacteria, the sludge was first washed thrice with sterilized 1 M HEPES [4-(2-hydroxyethyl)-1-piperazineethaesulfonic acid] buffer (pH 7.0), and then 10 ml of the same buffer was used to resuspend bacterial cells. Serially diluted samples (in the HEPES buffer) were plated on LB (Luria-Bertani) agar medium and incubated at 30 ± 2°C for 10 days. To isolate both slow and fast growers (to cover a wider range of bacterial communities), single colonies were selected at different time intervals (2, 4, 6, 8, and 10 days) and transferred to 96-well microtiter plates containing LB medium at 100 μl/well. In addition, EPS-producing strains were selected based on their mucoid colonies (54) and crystal violet staining (55). Finally, a total of 23 strains were isolated and stored in 25% (vol/vol) glycerol at −80°C for further experiments.

The genomic DNA of these 23 isolated bacteria was extracted individually for direct amplification of 16S rRNA gene portions (56) by PCR. The isolation of DNA was completed as per the manufacturer's instructions (Tiangen, Beijing, People's Republic of China). The primer set 27F (5′-AGA GTT TGA TCM TGG CTC AG-3′) and 1492R (5′-CGG TTA CCT TGT TAC GAC TT-3′) was used to amplify 16S rRNA gene fragments (57). Briefly, 0.5 μl of diluted DNA was added to a PCR tube containing 49.5 μl of PCR mixture (27F primer, 1.0 μl; 1492R primer, 1.0 μl; dinucleoside triphosphates [dNTPs], 5.0 μl; 5× Fast *PFU* buffer, 10.0 μl; Fast *PFU* polymerase, 1.0 μl; and distilled water, 31.5 μl). Then, the mixture was distributed equally into 3 PCR tubes for effective amplification. A thermal cycler (GeneAmp PCR system 9700; Applied Biosystems, CA, USA) was used for PCR amplification. Finally, amplified products were sent to BGI Genomics Co., Ltd. (Beijing Genomics Institute, Shenzhen, People's Republic of China) for sequence analysis. For the similarity search, the 16S rRNA gene sequences of the 23 strains were subjected to a BLAST search online (http://www.ncbi.nlm.nih.gov/BLAST).

Extraction of bound EPS. Bound EPS was extracted (58) by removing the SMPs via centrifuging the culture broth (25 ml from mid-stationary phase, i.e., 48 h) at 3,500 rpm and 4°C for 15 min. Then, a cell pellet with intact bound EPS was dissolved in a 0.5% NaCl solution (25 ml) and placed in a water bath at 60°C for 30 min. Afterward, the suspension was centrifuged again at 12,000 rpm and 4°C for 15 min, and the supernatant was considered to harbor bound EPS. The dry weight of the crude EPS (in grams per liter) was measured by drying at 105°C for 8 h (59). The concentrations of carbohydrate and protein in the EPS (in milligrams per liter) were analyzed using phenol-sulfuric acid (60) and modified Lowry methods (61), respectively. In addition, the EPS was purified by dialysis for 1 day against deionized (DI) water (4°C) and lyophilized at −50°C for 10 to 12 h in preparation for the following FTIR analysis. To fix the incubation time for the extraction of EPS, 3% (vol/vol) inoculum was used to inoculate 100 ml of a sterilized glucose-yeast extract medium (pH 7.4) (62), followed by incubation for 3 days at 30°C and 180 rpm. The composition of glucose-yeast extract medium was as follows (in grams per liter): glucose, 0.5; yeast extract, 0.5; $(NH_4)_2SO_4$, 0.5; NaCl, 0.1; K_2HPO_4, 5.0; and KH_2PO_4, 2.0. EPS dry weight and viable cell numbers (standard plate count method) of samples were measured at regular intervals (6, 12, 24, 36, 48, 60, and 72 h).

FTIR characterization and 2D-COS analysis of EPS-calcium interactions. An FTIR spectrometer (Nicolet 6700-Continuμm; Thermo Scientific Co., USA) was used to characterize the functional groups of EPS. The sample pellets were prepared by mixing the freeze-dried EPS powders with spectroscopy-grade potassium bromide (KBr) at a ratio of 1:100 prior to recording the spectra in an absorbance mode over a scan range of 400 to 4,000 cm^{-1} with a resolution of 2 cm^{-1}. To investigate the potential overlapping peaks in the spectra, the representative peaks at 900 to 960 cm^{-1} and 1,500 to 1,700 cm^{-1} were curve fitted using the Fourier deconvolution of Gaussian instrument response function from the PeakFit software (PeakFit version 4.12; Systat Software, Inc.) (63).

The changes in EPS functional groups in the presence of calcium were also studied. Specifically, EPS were first extracted from three selected strains, *Bacillus* sp. JSB10, *Proteus* sp. JSB20, and *Vagococcus* sp. JSB21. Then, EPS with a total organic carbon of 185 mg/liter was mixed with different concentrations of calcium (i.e., 0.1, 0.2, 0.3, 0.5, 0.6, 0.8, and 1.0 mM). Finally, the EPS-Ca^{2+} complexes were freeze-dried and subjected to FTIR characterization. In addition, 2D-FTIR-COS, including synchronous and asynchronous spectra, were also involved and analyzed according to Noda's method to further investigate the susceptibility of EPS functional groups to calcium (64).

Membrane filtration tests. Bacterial cells for the membrane filtration test were harvested from culture broth after 48 h of incubation with centrifugation at 3,500 rpm and 4°C for 15 min and washed twice in 0.9% NaCl solution. Then, 100 ml of cell suspension for each bacterial strain was

prepared for the membrane fouling evaluation experiments. The cell density (optical density at 600 nm [OD_{600}]) was maintained at 0.6 for all the suspensions. Membrane filtration tests were conducted using a dead-end stirred cell (MSC300; Mosu Co., Shanghai, China) with a volume of 300 ml and an effective surface area of 37.4 cm^2. Flat-sheet polyethersulfone membranes (RisingSun Membrane Technology Co., Ltd., Beijing, People's Republic of China) with a pore size of 0.1 μm were used. A constant pressure of 50 kPa was applied (type-10 CN-68825-00; Marsh Bellofram Co., Newell, WV, USA) throughout the filtration. The permeate flux was recorded automatically using an electronic balance (G&G E600Y-2; Neuss, Germany) through a data login system. To investigate the impact of calcium on the fouling potential of bacterial strains, three representative strains were employed (i.e., *Bacillus* sp. JSB10, *Proteus* sp. JSB20, and *Vagococcus* sp. JSB21 as the high-, medium-, and low-fouling bacteria, respectively). Two different Ca^{2+} concentrations (0.1 and 0.5 mM) were used. To maintain the same ionic strength (1.5 mM) in all the samples, 1.2 mM NaCl was added to the samples in addition to 0.1 mM Ca^{2+}. The unified membrane fouling index (UMFI) was applied to calculate the fouling extents of different bacteria (65).

Additional analyses. The viscosity of each cell suspension (~18 ml) was measured using a rheometer (DV III Ultra; Brookfield) at 25°C. The zeta potentials (ζ) of the cell suspensions were measured using a Zetasizer (Nano ZS90, Malvern Corp., UK). Statistical analysis was performed using the GraphPad Prism 7 software at a 95% confidence level ($P \leq 0.05$), unless otherwise stated. Two-way analysis of variance (ANOVA, Tukey's multiple-comparison test) and correlation analysis were performed to assess the statistical significance among the different treatments.

Accession number(s). The sequence data for each of 20 identified bacterial strains were deposited in GenBank, under accession numbers MG595640, MG595665, MG596916 to MG596923, MG596948 to MG596954, MG596967, MG596968, and MG603267 (see Table S7 in the supplemental material).

SUPPLEMENTAL MATERIAL

Supplemental material for this article may be found at https://doi.org/10.1128/AEM.00756-18.

SUPPLEMENTAL FILE 1, PDF file, 1.0 MB.

ACKNOWLEDGMENTS

This study benefited from grants from the Chinese Postdoctoral Science Foundation (grant 2017M612807), the National Natural Science Foundation of China (grants 51608546 and 51478487), and the Natural Science Foundation of Guangdong Province (grant 2014A030306002).

REFERENCES

1. Meng F, Zhang S, Oh Y, Zhou Z, Shin HS, Chae SR. 2017. Fouling in membrane bioreactors: an updated review. Water Res 114:151–180. https://doi.org/10.1016/j.watres.2017.02.006.
2. Neemann F, Rosenberger S, Jefferson B, McAdam EJ. 2013. Non-covalent protein-polysaccharide interactions and their influence on membrane fouling. J Memb Sci 446:310–317. https://doi.org/10.1016/j.memsci.2013.06.054.
3. Yu W, Graham N, Yang Y, Zhou Z, Campos LC. 2015. Effect of sludge retention on UF membrane fouling: the significance of sludge crystallization and EPS increase. Water Res 83:319–328. https://doi.org/10.1016/j.watres.2015.06.049.
4. Xin Y, Bligh MW, Kinsela AS, Waite TD. 2016. Effect of iron on membrane fouling by alginate in the absence and presence of calcium. J Memb Sci 497:289–299. https://doi.org/10.1016/j.memsci.2015.09.023.
5. Drews A. 2010. Membrane fouling in membrane bioreactors–characterisation, contradictions, cause and cures. J Memb Sci 363:1–28. https://doi.org/10.1016/j.memsci.2010.06.046.
6. Habimana O, Semião AJC, Casey E. 2014. The role of cell-surface interactions in bacterial initial adhesion and consequent biofilm formation on nanofiltration/reverse osmosis membranes. J Memb Sci 454:82–96. https://doi.org/10.1016/j.memsci.2013.11.043.
7. Lee W-N, Cheong W-S, Yeon K-M, Hwang B-K, Lee C-H. 2009. Correlation between local TMP distribution and bio-cake porosity on the membrane in a submerged MBR. J Memb Sci 332:50–55. https://doi.org/10.1016/j.memsci.2009.01.036.
8. Jo SJ, Kwon H, Jeong S-Y, Lee C-H, Kim TG. 2016. Comparison of microbial communities of activated sludge and membrane biofilm in 10 full-scale membrane bioreactors. Water Res 101:214–225. https://doi.org/10.1016/j.watres.2016.05.042.
9. Urbain V, Block JC, Manem J. 1993. Bioflocculation in activated sludge: an analytic approach. Water Res 27:829–838. https://doi.org/10.1016/0043-1354(93)90147-A.
10. Xiao K, Chen Y, Jiang X, Zhou Y. 2017. Evaluating filterability of different types of sludge by statistical analysis: the role of key organic compounds in extracellular polymeric substances. Chemosphere 170:233–241. https://doi.org/10.1016/j.chemosphere.2016.12.030.
11. Gutman J, Herzberg M, Walker SL. 2014. Biofouling of reverse osmosis membranes: positively contributing factors of *Sphingomonas*. Environ Sci Technol 48:13941–13950. https://doi.org/10.1021/es503680s.
12. Herzberg M, Kang S, Elimelech M. 2009. Role of extracellular polymeric substances (EPS) in biofouling of reverse osmosis membranes. Environ Sci Technol 43:4393–4398. https://doi.org/10.1021/es900087j.
13. Wang Z, Wu Z, Tang S. 2009. Extracellular polymeric substances (EPS) properties and their effects on membrane fouling in a submerged membrane bioreactor. Water Res 43:2504–2512. https://doi.org/10.1016/j.watres.2009.02.026.
14. Arabi S, Nakhla G. 2008. Impact of protein/carbohydrate ratio in the feed wastewater on the membrane fouling in membrane bioreactors. J Memb Sci 324:142–150. https://doi.org/10.1016/j.memsci.2008.07.026.
15. Liu Q, Qiu G, Zhou Z, Li J, Amy GL, Xie J, Lee JY. 2016. An effective design of electrically conducting thin-film composite (TFC) membranes for bio and organic fouling control in forward osmosis (FO). Environ Sci Technol 50:10596–10605. https://doi.org/10.1021/acs.est.6b03402.
16. Yoshida K, Tashiro Y, May T, Okabe S. 2015. Impacts of hydrophilic colanic acid on bacterial attachment to microfiltration membranes and subsequent membrane biofouling. Water Res 76:33–42. https://doi.org/10.1016/j.watres.2015.02.045.
17. Lee H-J, Kim H-E, Lee C. 2017. Combination of cupric ion with hydroxylamine and hydrogen peroxide for the control of bacterial biofilms on

RO membranes. Water Res 110:83–90. https://doi.org/10.1016/j.watres.2016.12.014.
18. Chen W, Liu XY, Huang BC, Wang LF, Yu HQ, Mizaikoff B. 2016. Probing membrane fouling via infrared attenuated total reflection mapping coupled with multivariate curve resolution. Chemphyschem 17:358–363. https://doi.org/10.1002/cphc.201500932.
19. Flemming HC, Leis A. 2002. Sorption properties of biofilms, p 2958–2967. *In* Bitton G (ed), Encyclopedia of environmental microbiology. John Wiley & Sons, Inc., New York, NY.
20. Badireddy AR, Korpol BR, Chellam S, Gassman PL, Engelhard MH, Lea AS, Rosso KM. 2008. Spectroscopic characterization of extracellular polymeric substances from *Escherichia coli* and *Serratia marcescens*: suppression using sub-inhibitory concentrations of bismuth thiols. Biomacromolecules 9:3079–3089. https://doi.org/10.1021/bm800600p.
21. Chen Y-P, Zhang P, Guo J-S, Fang F, Gao X, Li C. 2013. Functional groups characteristics of EPS in biofilm growing on different carriers. Chemosphere 92:633–638. https://doi.org/10.1016/j.chemosphere.2013.01.059.
22. Yuan S-J, Sun M, Sheng G-P, Li Y, Li W-W, Yao R-S, Yu H-Q. 2011. Identification of key constituents and structure of the extracellular polymeric substances excreted by *Bacillus megaterium* TF10 for their flocculation capacity. Environ Sci Technol 45:1152–1157. https://doi.org/10.1021/es1030905.
23. Hou X, Liu S, Zhang Z. 2015. Role of extracellular polymeric substance in determining the high aggregation ability of anammox sludge. Water Res 75:51–62. https://doi.org/10.1016/j.watres.2015.02.031.
24. Meng F, Liao B, Liang S, Yang F, Zhang H, Song L. 2010. Morphological visualization, componential characterization and microbiological identification of membrane fouling in membrane bioreactors (MBRs). J Memb Sci 361:1–14. https://doi.org/10.1016/j.memsci.2010.06.006.
25. Flemming H-C, Wingender J. 2010. The biofilm matrix. Nat Rev Microbiol 8:623–633. https://doi.org/10.1038/nrmicro2415.
26. Badireddy AR, Chellam S, Gassman PL, Engelhard MH, Lea AS, Rosso KM. 2010. Role of extracellular polymeric substances in bioflocculation of activated sludge microorganisms under glucose-controlled conditions. Water Res 44:4505–4516. https://doi.org/10.1016/j.watres.2010.06.024.
27. Cetin Z, Kantar C, Alpaslan M. 2009. Interactions between uronic acids and chromium(III). Environ Toxicol Chem 28:1599–1608. https://doi.org/10.1897/08-654.1.
28. Kim IS, Jang N. 2006. The effect of calcium on the membrane biofouling in the membrane bioreactor (MBR). Water Res 40:2756–2764. https://doi.org/10.1016/j.watres.2006.03.036.
29. Hu M, Zheng S, Mi B. 2016. Organic fouling of graphene oxide membranes and its implications for membrane fouling control in engineered osmosis. Environ Sci Technol 50:685–693. https://doi.org/10.1021/acs.est.5b03916.
30. Khan R, Shen F, Khan K, Liu LX, Wu HH, Luo JQ, Wan YH. 2016. Biofouling control in a membrane filtration system by a newly isolated novel quorum quenching bacterium, *Bacillus methylotrophicus* sp. WY. RSC Adv 6:28895–28903. https://doi.org/10.1039/C6RA01663D.
31. Badireddy AR, Chellam S, Yanina S, Gassman P, Rosso KM. 2008. Bismuth dimercaptopropanol (BisBAL) inhibits the expression of extracellular polysaccharides and proteins by *Brevundimonas diminuta*: implications for membrane microfiltration. Biotechnol Bioeng 99:634–643. https://doi.org/10.1002/bit.21615.
32. Maruyama T, Katoh S, Nakajima M, Nabetani H, Abbott TP, Shono A, Satoh K. 2001. FT-IR analysis of BSA fouled on ultrafiltration and microfiltration membranes. J Memb Sci 192:201–207. https://doi.org/10.1016/S0376-7388(01)00502-6.
33. Sheng G-P, Xu J, Luo H-W, Li W-W, Li W-H, Yu H-Q, Xie Z, Wei S-Q, Hu F-C. 2013. Thermodynamic analysis on the binding of heavy metals onto extracellular polymeric substances (EPS) of activated sludge. Water Res 47:607–614. https://doi.org/10.1016/j.watres.2012.10.037.
34. Bramhachari PV, Dubey SK. 2006. Isolation and characterization of exopolysaccharide produced by *Vibrio harveyi* strain VB23. Lett Appl Microbiol 43:571–577. https://doi.org/10.1111/j.1472-765X.2006.01967.x.
35. Ishizaki S, Fukushima T, Ishii S, Okabe S. 2016. Membrane fouling potentials and cellular properties of bacteria isolated from fouled membranes in a MBR treating municipal wastewater. Water Res 100:448–457. https://doi.org/10.1016/j.watres.2016.05.027.
36. Xin Y, Bligh MW, Kinsela AS, Wang Y, Waite TD. 2015. Calcium-mediated polysaccharide gel formation and breakage: impact on membrane foulant hydraulic properties. J Memb Sci 475:395–405. https://doi.org/10.1016/j.memsci.2014.10.033.
37. Patrauchan MA, Sarkisova S, Sauer K, Franklin MJ. 2005. Calcium influences cellular and extracellular product formation during biofilm-associated growth of a marine *Pseudoalteromonas* sp. Microbiology 151:2885–2897. https://doi.org/10.1099/mic.0.28041-0.
38. Ang WS, Elimelech M. 2007. Protein (BSA) fouling of reverse osmosis membranes: implications for wastewater reclamation. J Memb Sci 296:83–92. https://doi.org/10.1016/j.memsci.2007.03.018.
39. Ferrando D, Toubiana D, Kandiyote NS, Nguyen TH, Nejidat A, Herzberg M. 2018. Ambivalent role of calcium in the viscoelastic properties of extracellular polymeric substances and the consequent fouling of reverse osmosis membranes. Desalination 429:12–19. https://doi.org/10.1016/j.desal.2017.12.006.
40. Seviour T, Yuan Z, van Loosdrecht MC, Lin Y. 2012. Aerobic sludge granulation: a tale of two polysaccharides? Water Res 46:4803–4813. https://doi.org/10.1016/j.watres.2012.06.018.
41. Wiercigroch E, Szafraniec E, Czamara K, Pacia MZ, Majzner K, Kochan K, Kaczor A, Baranska M, Malek K. 2017. Raman and infrared spectroscopy of carbohydrates: a review. Spectrochim Acta A Mol Biomol Spectrosc 185:317–335. https://doi.org/10.1016/j.saa.2017.05.045.
42. Xiao Q, Gu X, Tan S. 2014. Drying process of sodium alginate films studied by two-dimensional correlation ATR-FTIR spectroscopy. Food Chem 164:179–184. https://doi.org/10.1016/j.foodchem.2014.05.044.
43. Vu B, Chen M, Crawford RJ, Ivanova EP. 2009. Bacterial extracellular polysaccharides involved in biofilm formation. Molecules 14:2535–2554. https://doi.org/10.3390/molecules14072535.
44. Lee K, Lee K-M, Kim D, Yoon SS. 2017. Molecular determinants of the matrix thickening of a dual-species *Pseudomonas aeruginosa* and *Enterococcus faecalis* biofilm. Appl Environ Microbiol https://doi.org/10.1128/AEM.01182-17.
45. Lee IC, Caggianiello G, van Swam II, Taverne N, Meijerink M, Bron PA, Spano G, Kleerebezem M. 2016. Strain-specific features of extracellular polysaccharides and their impact on *Lactobacillus plantarum*-host interactions. Appl Environ Microbiol 82:3959–3970. https://doi.org/10.1128/AEM.00306-16.
46. Xiao K, Chen Y, Jiang X, Tyagi VK, Zhou Y. 2016. Characterization of key organic compounds affecting sludge dewaterability during ultrasonication and acidification treatments. Water Res 105:470–478. https://doi.org/10.1016/j.watres.2016.09.030.
47. Okamura D, Mori Y, Hashimoto T, Hori K. 2009. Identification of biofoulant of membrane bioreactors in soluble microbial products. Water Res 43:4356–4362. https://doi.org/10.1016/j.watres.2009.06.042.
48. Nivens DE, Ohman DE, Williams J, Franklin MJ. 2001. Role of alginate and its *O* acetylation in formation of *Pseudomonas aeruginosa* microcolonies and biofilms. J Bacteriol 183:1047–1057. https://doi.org/10.1128/JB.183.3.1047-1057.2001.
49. Delille A, Quiles F, Humbert F. 2007. *In situ* monitoring of the nascent *Pseudomonas fluorescens* Biofilm response to variations in the dissolved organic carbon level in low-nutrient water by attenuated total reflectance-Fourier transform infrared spectroscopy. Appl Environ Microbiol 73:5782–5788. https://doi.org/10.1128/AEM.00838-07.
50. Omoike A, Chorover J. 2004. Spectroscopic study of extracellular polymeric substances from *Bacillus subtilis*: aqueous chemistry and adsorption effects. Biomacromolecules 5:1219–1230. https://doi.org/10.1021/bm034461z.
51. Lin H, Zhang M, Wang F, Meng F, Liao B-Q, Hong H, Chen J, Gao W. 2014. A critical review of extracellular polymeric substances (EPSs) in membrane bioreactors: characteristics, roles in membrane fouling and control strategies. J Memb Sci 460:110–125. https://doi.org/10.1016/j.memsci.2014.02.034.
52. Xu H, Yang C, Jiang H. 2016. Aggregation kinetics of inorganic colloids in eutrophic shallow lakes: influence of cyanobacterial extracellular polymeric substances and electrolyte cations. Water Res 106:344–351. https://doi.org/10.1016/j.watres.2016.10.023.
53. Li QL, Elimelech M. 2004. Organic fouling and chemical cleaning of nanofiltration membranes: measurements and mechanisms. Environ Sci Technol 38:4683–4693. https://doi.org/10.1021/es0354162.
54. Bala Subramanian S, Yan S, Tyagi RD, Surampalli RY. 2010. Extracellular polymeric substances (EPS) producing bacterial strains of municipal wastewater sludge: isolation, molecular identification, EPS characterization and performance for sludge settling and dewatering. Water Res 44:2253–2266. https://doi.org/10.1016/j.watres.2009.12.046.
55. Cain D, Hanks H, Weis M, Bottoms C, Lawson J. 2009. Microbiology laboratory manual. Collin County Community College District, McKinney, TX.
56. Widmer F, Seidler RJ, Gillevet PM, Watrud LS, Di Giovanni GD. 1998. A

highly selective PCR protocol for detecting 16S rRNA genes of the genus *Pseudomonas* (*sensu stricto*) in environmental samples. Appl Environ Microbiol 64:2545–2553.
57. Stackebrandt E, Goodfellow M. 1991. Nucleic acid techniques in bacterial systematics. Wiley, Chichester, United Kingdom.
58. Zhang X, Bishop PL, Kinkle BK. 1999. Comparison of extraction methods for quantifying extracellular polymers in biofilms. Water Sci Technol 39:211–218. https://doi.org/10.1016/S0273-1223(99)00170-5.
59. APHA. 2005. Standard methods for the examination of water and wastewater, 21st ed. American Public Health Association, Washington, DC.
60. DuBois M, Gilles KA, Hamilton JK, Rebers PA, Smith F. 1956. Colorimetric method for determination of sugars and related substances. Anal Chem 28:350–356. https://doi.org/10.1021/ac60111a017.
61. Hartree EF. 1972. Determination of protein: a modification of the Lowry method that gives a linear photometric response. Anal Biochem 48:422–427. https://doi.org/10.1016/0003-2697(72)90094-2.
62. Bezawada J, Hoang NV, More TT, Yan S, Tyagi N, Tyagi RD, Surampalli RY. 2013. Production of extracellular polymeric substances (EPS) by *Serratia* sp.1 using wastewater sludge as raw material and flocculation activity of the EPS produced. J Environ Manag 128:83–91. https://doi.org/10.1016/j.jenvman.2013.04.039.
63. Yin C, Meng F, Chen GH. 2015. Spectroscopic characterization of extracellular polymeric substances from a mixed culture dominated by ammonia-oxidizing bacteria. Water Res 68:740–749. https://doi.org/10.1016/j.watres.2014.10.046.
64. Noda I. 2004. Advances in two-dimensional correlation spectroscopy. Vibrat Spectrosc 36:143–165. https://doi.org/10.1016/j.vibspec.2003.12.016.
65. Huang H, Young TA, Jacangelo JG. 2008. Unified membrane fouling index for low pressure membrane filtration of natural waters: principles and methodology. Environ Sci Technol 42:714–720. https://doi.org/10.1021/es071043j.
66. Synytsya A, Novák M. 2013. Structural diversity of fungal glucans. Carbohydr Polym 92:792–809. https://doi.org/10.1016/j.carbpol.2012.09.077.